The Journal of the Anti-Seismic Systems International Society (ASSISi)

Seismic Isolation and Protection Systems

STABILITY AND POST-BUCKLING BEHAVIOR IN NONBOLTED ELASTOMERIC ISOLATORS

James M. Kelly and Maria Rosaria Marsico

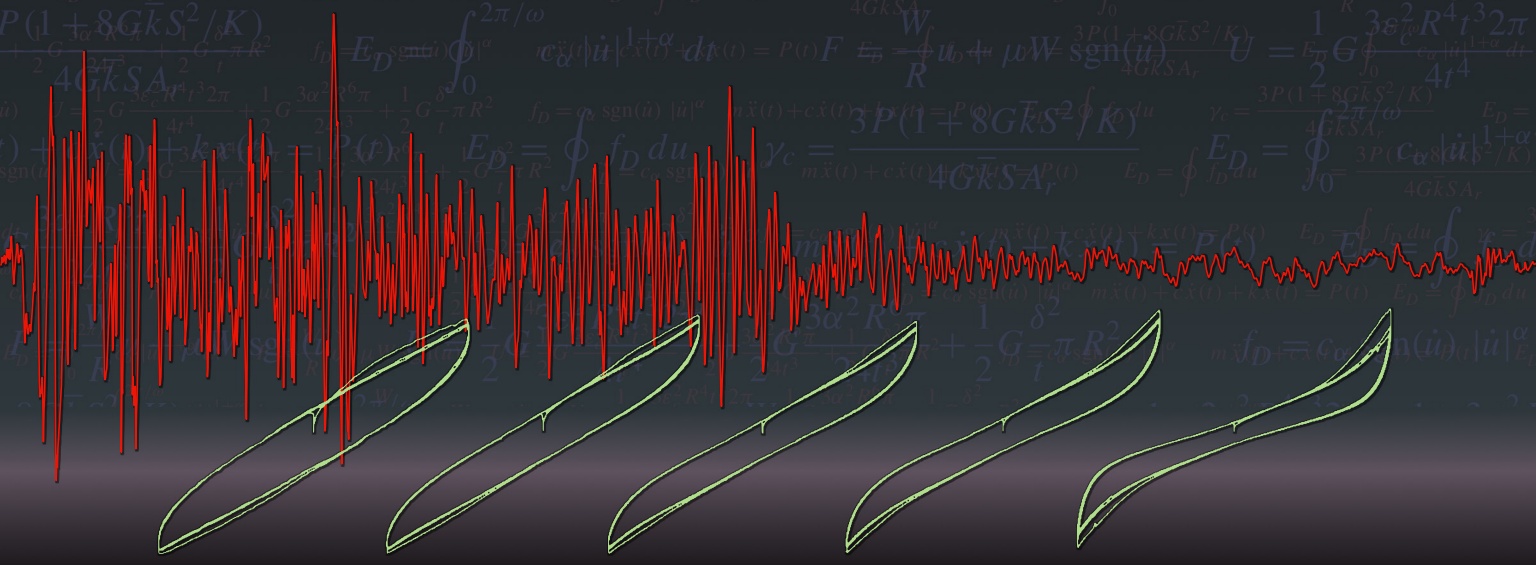

vol 1, no 1 2010

mathematical sciences publishers

mathematical sciences publishers + Anti-Seismic Systems International Society
SEISMIC ISOLATION AND PROTECTION SYSTEMS 1:1 (2010)

STABILITY AND POST-BUCKLING BEHAVIOR IN NONBOLTED ELASTOMERIC ISOLATORS

JAMES M. KELLY AND MARIA ROSARIA MARSICO

This paper is a theoretical and numerical study of the stability of light-weight low-cost elastomeric isolators for application to housing, schools and other public buildings in highly seismic areas of the developing world. The theoretical analysis covers the buckling of multilayer elastomeric isolation bearings where the reinforcing elements, normally thick and inflexible steel plates, are replaced by thin flexible reinforcement. The reinforcement in these bearings, in contrast to the steel in the conventional isolator (which is assumed to be rigid both in extension and flexure), is assumed to be completely without flexural rigidity. This is of course not completely accurate but allows the determination of a lower bound to the ultimate buckling load of the isolator. In addition, there are fewer reinforcing layers than in conventional isolators which makes them lighter but the most important aspect of these bearings is that they do not have end plates again reducing the weight but also they are not bonded to the upper and lower support surfaces. The intention of the research program of which this study is a part is to provide a low-cost light-weight isolation system for housing and public buildings in developing countries.

1. Introduction

The recent earthquakes in India, Turkey and South America have again emphasized the fact that the major loss of life in earthquakes happens when the event occurs in developing countries. Even in relatively moderate earthquakes in areas with poor housing many people are killed by the collapse of brittle heavy unreinforced masonry or poorly constructed concrete buildings. Modern structural control technologies such as active control or energy dissipation devices can do little to alleviate this but it is possible that seismic isolation could be adapted to improve the seismic resistance of poor housing and other buildings such as schools and hospitals in developing countries [Kelly 2002].

The theoretical basis of seismic isolation [Kelly 1997] shows that the reduction of seismic loading produced by the isolation systems depends primarily on the ratio of the isolation period to the fixed base period. Since the fixed base period of a masonry block or brick building may be of the order of 0.1 second, an isolation period of 1 sec. or longer would provide a significant reduction in the seismic loads on the building and would not require a large isolation displacement. For example, the current UBC code for seismic isolation [UBC 2007, Chapters 16, 17] has a formula for minimum isolator displacement which, for a 1.5 second system, would be around 15 cm (6 inches).

The problem with adapting isolation to developing countries is that conventional isolators are large, expensive, and heavy. An individual isolator can weight one ton or more and cost as much as $10,000 for each isolator. To extend this valuable earthquake-resistant strategy to housing and commercial buildings, it is necessary to reduce the cost and weight of the isolators.

Keywords: elastomeric bearings, low-cost isolation system, instability, nonbolted multilayer rubber bearing, buckling, roll-out.

The primary weight in an isolator is due to the steel reinforcing plates, which are used to provide the vertical stiffness of the rubber-steel composite element. A typical rubber isolator has two large end-plates (25 mm) and 20 thin reinforcing plates (3 mm). The high cost of producing the isolators results from the labor involved in preparing the steel plates and the laying-up of the rubber sheets and steel plates for vulcanization bonding in a mold. The steel plates are cut, sand-blasted, acid cleaned, and then coated with bonding compound. Next, the compounded rubber sheets with the interleaved steel plates are put into a mold and heated under pressure for several hours to complete the manufacturing process. The purpose of this program of the research of which this is a part is to suggest that both the weight and the cost of isolators can be reduced by using fiber reinforcing sheets [Kelly 1999], no end plates and no bonding to the support surfaces. Since the demands on the bonding between the rubber and the reinforcing plates are reduced, a simpler and less expensive manufacturing process can be used.

The manufacturing process for conventional isolators has to be done very carefully because the testing requirements in the current codes for seismic isolation require that the isolators be tested prior to use for very extreme loading conditions. The bond between the rubber and the steel reinforcement and between the rubber and the end plates must be very good for the bearing to survive these tests [Gent and Meinecke 1970]. The effect of a large shear displacement of the isolator is to generate an unbalanced moment that must be balanced by tensile stresses. The compression load is carried through the overlap region between top and bottom surfaces and the unbalanced moment is carried by tension stresses in the regions outside the overlap as shown in the diagram in Figure 1.

The bearings being studied here do not have these tension stresses. The primary reason for this is the fact that the top and bottom surfaces can roll off the support surfaces and no tension stresses are produced. The unbalanced moments are resisted by the vertical load through offset of the force resultants on the top and bottom surfaces.

While these isolators can undergo large displacements there is a concern with their stability. The conventional analysis for the buckling of isolators has focused only on isolators that are bolted at each end to rigid surfaces [Imbimbo and Kelly 1997]. The analysis is also based on the assumption that the steel reinforcing plates are essentially rigid but here the shims are very thin and bending of the shims could have an effect on the stability of these bearings [UBC 2007]. In this paper we will study the

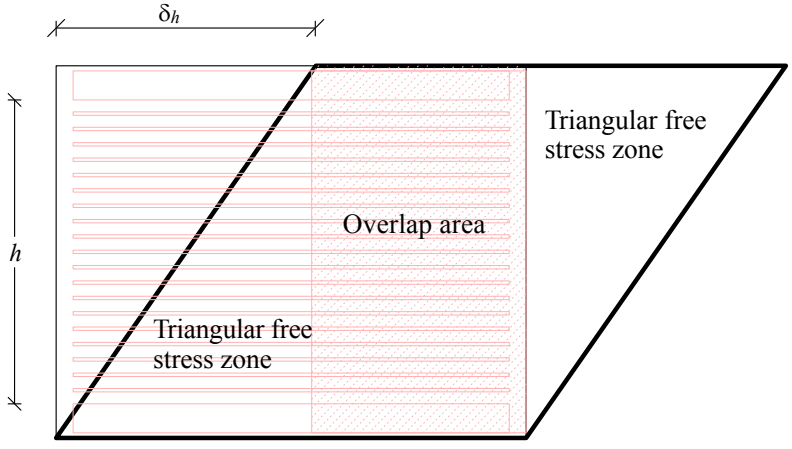

Figure 1. Overlap area between the top and bottom of the bearing.

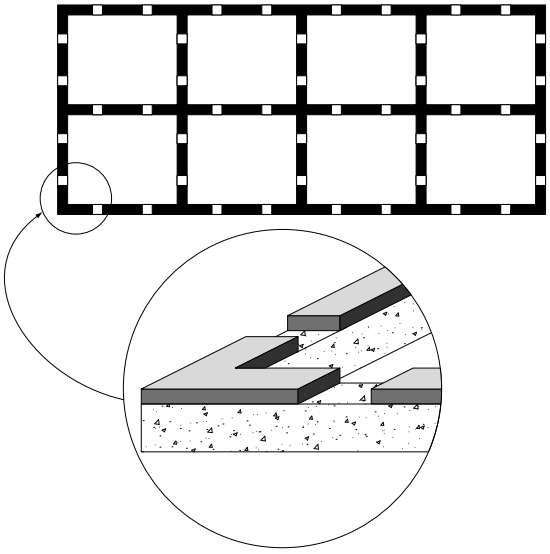

Figure 2. System of strip isolators in wall building.

buckling of such a bearing and attempt to clarify the post-buckling behavior based on the postulate that the vertical load in the buckled configuration is carried through the overlap area between top and bottom and that the triangular areas outside the overlap area are free of stresses. The approach will be done first for a bearing in the form of an infinite strip and then will be applied to a circular bearing. One reason for studying the strip is that the solution can be easily checked by a two-dimensional numerical model which might be considered as an experimental test.

Another benefit to using fiber reinforcement is that it would then be possible to build isolators in long rectangular strips, whereby individual isolators could be cut to the required size [Kelly and Takhirov 2002]. All isolators are currently manufactured as either circular or square. Rectangular isolators in the form of long strips would have distinct advantages over square or circular isolators when applied to buildings where the lateral resisting system is walls. When isolation is applied to buildings with structural walls, additional wall beams are needed to carry the wall from isolator to isolator. A strip isolator would have a distinct advantage for retrofitting masonry structures and for isolating residential housing constructed from concrete or masonry blocks. A possible layout of a complete system of strip isolators is shown in Figure 2.

2. Theoretical underpinnings of the stability analysis

The theoretical analysis is concerned with the buckling of a long strip bearing in which the stress state is essentially plain strain as shown in Figure 4; see [Kelly 2003]. When the bearing is displaced horizontally the material begins to roll-off the supports and the vertical load is carried through the overlap area between the top and bottom of the bearing as shown in Figure 3 and Figure 1. Thus the effective column cross-sectional area is reduced and the buckling load and the vertical stiffness are reduced also. The bearing shown in Figure 4 is a long strip fiber-reinforced bearing under vertical load and displaced horizontally to a shear deformation of 100% shear strain in its short direction [Tsai and Kelly 2002]. The fiber sheets

Figure 3. Fiber-reinforced strip bearing under vertical load and horizontal displacement test.

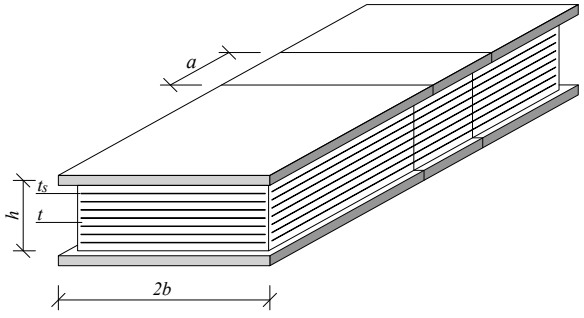

Figure 4. An infinite strip pad of width $2b$.

are distinctly shown in the figure and it is clear that they are flat in the region of overlap between top and bottom. It is the postulate of this analysis that the vertical load is carried through the overlap area in the same way as a conventionally reinforced bearing and that the two triangular regions under the roll-off are stress free.

The process can be visualized as being conducted in a displacement controlled test machine where a steadily increasing vertical displacement is imposed on the bearing. At the first stage the vertical force needed to produce the displacement rises until the load reaches the buckling load whereupon the bearing begins to buckle sideways and to roll-off at the ends, thus reducing the effective area.

To determine the relationship between the imposed vertical displacement and the resulting horizontal displacement we use a relationship developed to analyze the interaction between the vertical stiffness and the horizontal displacement of a bearing using the linear elastic equations for a multilayer elastomer bearing. This result from [Tsai and Kelly 2005a]. provides the vertical displacement resulting from a horizontal displacement of the top of a bearing, this being in addition to that caused directly by vertical compression due to the axial load. This additional vertical displacement we will call the geometric part of displacement and denote it by δ_v^G and the connection between this and the horizontal displacement is given in [UBC 2007] as

$$\delta_v^G = \frac{\pi G A_s}{4 P_{\text{crit}}} \left(\frac{\pi p - \sin \pi p}{1 - \cos \pi p} \right) \frac{\delta_h^2}{h}, \tag{2-1}$$

where $p = P/P_{\text{crit}}$, with P the applied vertical load and $P_{\text{crit}} = (\pi/h)(EI_s GA_s)^{1/2}$, leading to

$$\delta_v^G = \frac{1}{4}\left(\frac{GA_s}{EI_s}\right)^{1/2}\left(\frac{\pi p - \sin \pi p}{1 - \cos \pi p}\right)\delta_h^2. \tag{2-2}$$

In the first instance to model the two-dimensional numerical experiment the analysis will be based on an infinite strip with width $2b$, rubber layer thickness t and n rubber layers for a total height $h = nt + (n-1)t_s$, where t_s is the thickness of the reinforcing elements (Figure 4).

The compression modulus of a single pad in the form of a long strip is

$$E_c = 4GS^2, \tag{2-3}$$

where the shape factor is $S = b/t$ and the vertical stiffness of the whole bearing is

$$K_v = \frac{4GS^2(2b)}{nt}. \tag{2-4}$$

The two quantities GA_s and EI_s are the effective shear stiffness per unit length and the effective bending stiffness per unit length of the bearing modeled as a continuous homogeneous beam and are given by $GA_s = G(2b)h/nt$ and

$$EI_s = 4GS^2\frac{1}{5}\left(\frac{2}{3}b^2\right)\frac{h}{nt};$$

see [Kelly and Takhirov 2004]. This leads to the buckling load in the undeflected configuration as

$$P_{\text{crit}} = \frac{4\pi Gb^3}{\sqrt{15}\,nt^2}. \tag{2-5}$$

The vertical displacement due to pure compression of the bearing in the undeflected configuration, denoted by δ_v^C, corresponding to this load is

$$\delta_v^C = \frac{P_{\text{crit}}}{K_v} = \frac{\pi}{2\sqrt{15}}t. \tag{2-6}$$

It is quite unexpected that this displacement depends only on the thickness of a single layer. Since the dimension b cancels in this calculation, this means that if the width $2b$ is replaced by the overlap area when the bearing displaces sideways, namely $2b - \delta_h$, the compressive part of the vertical displacement remains unchanged. When the imposed vertical displacement is increased beyond $\pi t/(2\sqrt{15})$, the additional vertical displacement must be accommodated by a geometric displacement related to the horizontal deformation of the column as a whole [Marsico 2008]. The relation between the horizontal displacement and the geometrical part of the vertical displacement in terms of the stiffness quantities for the long strip reduces to

$$\delta_v^G = \frac{\pi\sqrt{15}}{16}\frac{t}{b^2}\delta_h^2. \tag{2-7}$$

This result is the geometric part of the vertical deflection of the bearing when it is displaced horizontally at the buckling load but it can be used to provide the horizontal displacement due to increased vertical displacement in the test machine by replacing $2b$ by the reduced area $2b - \delta_h$, giving

$$\frac{\delta_h^2}{(b - \delta_h/2)^2} = \frac{16}{\pi\sqrt{15}t}\left(\delta_v - \frac{\pi}{2\sqrt{15}}t\right). \tag{2-8}$$

The solution for $\delta_h/(2b)$ is

$$\frac{\delta_h}{2b} = \frac{\sqrt{\frac{2}{15}}(x-1)^{1/2}}{1+\sqrt{\frac{2}{15}}(x-1)^{1/2}}, \tag{2-9}$$

where

$$x = \frac{\delta_v}{\pi t/2\sqrt{15}}. \tag{2-10}$$

Substitution of this result back into the expression for P_{crit} based on the reduced area, denoted by $P_{\text{crit}}(\delta_h)$, and normalization by the value of P_{crit} based on the original area P^0_{crit} leads to

$$\frac{P_{\text{crit}}(\delta_h)}{P_{\text{crit}}} = p(\delta_h) = \left(1-\frac{\delta_h}{2b}\right)^3, \tag{2-11}$$

which, after substitution of the result for $\delta_h/(2b)$, reduces to

$$p(\delta_h) = \left(1+\sqrt{\tfrac{2}{15}}(x-1)^{1/2}\right)^{-3}. \tag{2-12}$$

The interesting point about this result is that it suggests that the buckling of the unbonded isolator is an example of classical imperfection sensitive buckling. The slope of the force displacement curve at the point of instability is negative infinity. The approximation of the post-buckling load immediately after buckling is

$$p(\delta_h) = 1 - 3\sqrt{\tfrac{2}{15}}(x-1)^{1/2}. \tag{2-13}$$

The post-buckling load, due the negatively infinite derivative just after buckling, drops very aggressively.

3. Numerical experiment

The analysis given in the previous section was based on the idea that the isolator is placed in a displacement controlled test machine and subjected to a steadily increasing vertical displacement which was denoted there by δ_v. This displacement manifests itself in the bearing in two parts, the first which is due to the axial shortening of the bearing due to pure compression and denoted by δ_v^C and the second due to the end shortening when the load reaches the critical load denoted by δ_v^G. When the displacement at which the load reaches the critical load is further increased the bearing can accommodate the increased vertical displacement by lateral displacement and this lateral displacement denoted there by δ_h can be calculated from the end shortening part of the total vertical displacement. To verify that this approach is at least qualitatively correct a finite element analysis was carried out on a simple model of a long strip isolator.

The numerical experiment was done using the finite element program MARC [1988]. The model is two-dimensional, corresponding to a long strip isolator and the reinforcing plates are modeled by rebar elements which have an axial stiffness but no bending resistance. This is an extreme case of plate flexibility but it is used to simplify the numerical analysis. The model has contact elements at the top and bottom surfaces that allow it roll off the rigid supports and a small horizontal load is applied at the

top to act as an imperfection and cause it to displace to one side when the load gets close to the buckling load [Tsai and Kelly 2005b].

The result is shown in the sequence of diagrams in Figure 5. The zone at the top where the surface has lost contact is directly above the bottom corner and the same in reverse at the bottom. The two triangular regions below and above the two roll out areas are free of stresses. When the vertical load is plotted against the vertical displacement as shown in Figure 6 the load rises linearly until it gets close to the buckling load then levels and then as the increased vertical displacement causes lateral displacement to develop the vertical load decreases with the reduction in the overlap area between the top and the bottom of the bearing. In effect the column is buckling with a steadily decreasing cross-sectional area. This then is, at least qualitatively, the behavior that we will attempt to reproduce analytically for a strip bearing and a circular bearing in the next two sections.

4. Vertical displacement of the top of a bearing for an infinite strip

The total vertical displacement on the top of the bearing is equal to the sum of the vertical displacement depending on the geometry and the one depending on the applied load as $\delta_v^t = \delta_v^G + \delta_v^0$. In particular the value of $\delta_v^0 = Ph/EA_s$ for an infinite strip is

$$\delta_v^0 = \frac{Pt_r t^2}{8Gb^3}. \tag{4-1}$$

The analysis of the experimental behavior of the bearing can be subdivided into three steps. First the lateral displacement, δ_h, is not present and the vertical load, P, with $0 \le P < P_{\text{crit}}$, is applied (Figure 7, left). As P grows it becomes equal to the critical load on the total area (Figure 7, middle); at this point the horizontal displacement, δ_h, begins to develop and the vertical load, P, is then the critical load calculated on the reduced area (Figure 7, right). See [Marsico and Kelly 2009].

When the horizontal displacement is not applied, the vertical displacement depending on the geometry (as in steps 1 and 2) is equal to 0; then the total vertical displacement is

$$\delta_v^t = 0 + \frac{Pt_r t^2}{8Gb^3} = \frac{Pt_r t^2}{8Gb^3}. \tag{4-2}$$

However, the displacement depending on the load changes from step 1 to step 2, because of the increasing load. Thus the total vertical displacement in step 2 is

$$\delta_v^t = 0 + \frac{\pi t}{2\sqrt{15}} = \frac{\pi t}{2\sqrt{15}}. \tag{4-3}$$

In step 3, the shortening on the top of the bearing will depend on the horizontal displacement and on the reduced area and will be

$$\delta_v^t = \frac{\pi}{16}\frac{t}{(b-\delta_h/2)^2}\sqrt{15}\,\delta_h^2 + \frac{\pi t}{2\sqrt{15}}. \tag{4-4}$$

Introducing

$$x = \frac{\delta_h}{2b} \quad \text{and} \quad \frac{P_{\text{crit}(Ar)}}{P_{\text{crit}}} = \left(1 - \frac{\delta_h}{2b}\right)^3 = (1-x)^3 = y_2,$$

for $x \geq 0$ and $\delta = \pi t/2\sqrt{15}$, we can plot $y_1 = \delta_v^t/(2b) = \delta\big(1 + \frac{15}{4}x^2(1-x)^2\big)$ versus y_2 and $y_1 = \delta_v^t/(2b)$ versus x. The behavior of the bearing is clarified in Figure 8, where the solid line represents the critical load increasing versus the vertical displacement produced while the dash line plots the horizontal displacement causing the critical load to decrease because the reduction of the area. The ratio w_c is defined as the critical load applied on the reduced area normalized with respect to the critical load on the total area.

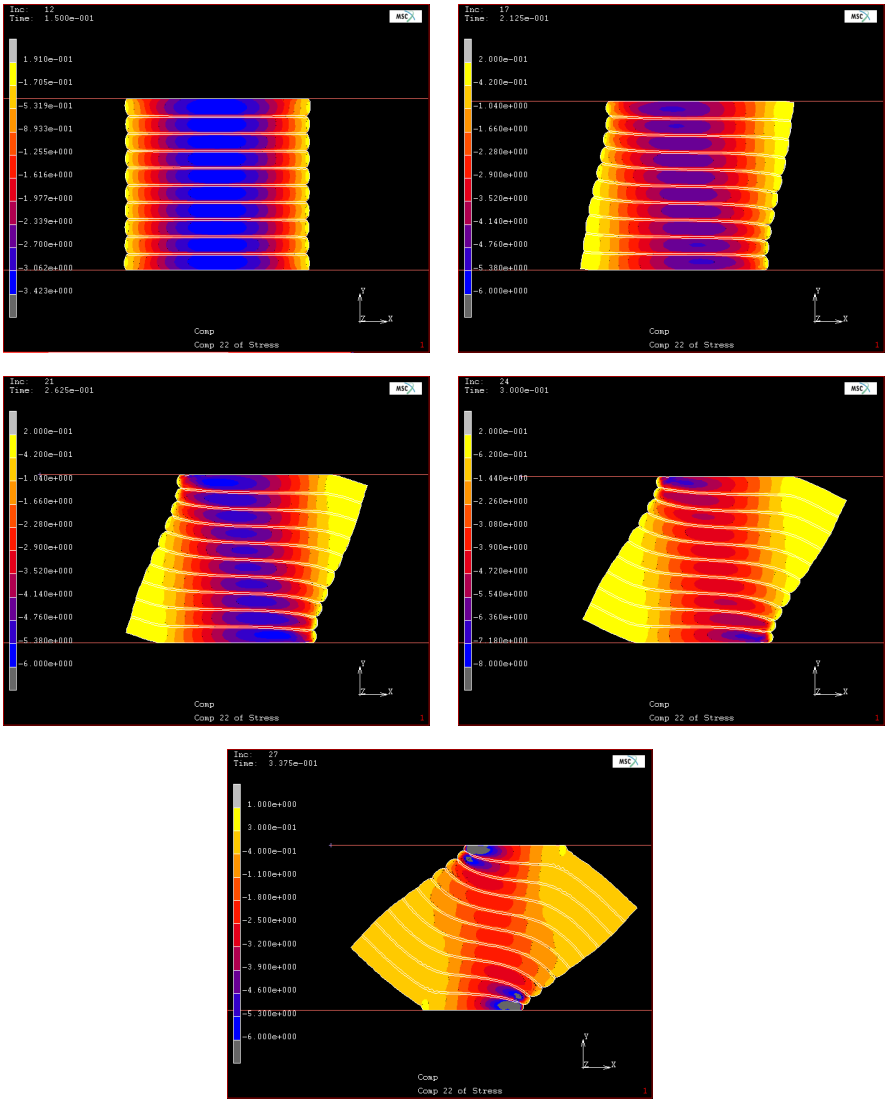

Figure 5. Sequence of buckling and post-buckling configurations showing stress-free triangular zones.

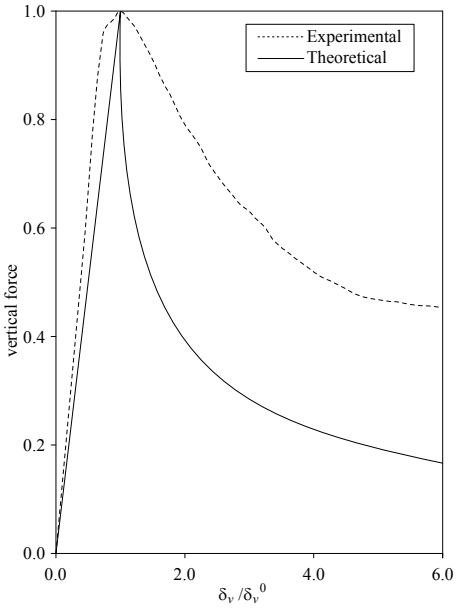

Figure 6. Normalized vertical force versus normalized vertical displacement from numerical experiment and analytical model.

5. Application of post-buckling analysis to circular bearing

Although the strip isolator has been suggested as the preferred form use with low-cost housing in developing countries there may be cases where it may be more convenient to use a circular isolator. For a circular bearing of radius R the parameters that differ from those of the strip bearing are the compression modulus E_c, the shape factor S and the effective moment of inertia I_{eff}. The modulus is

$$E_c = 6GS^2, \tag{5-1}$$

where the shape factor S is $R/(2t)$. The bending stiffness EI_{eff} in this case is

$$EI_{\text{eff}} = E_c\left(\tfrac{1}{3}I\right), \tag{5-2}$$

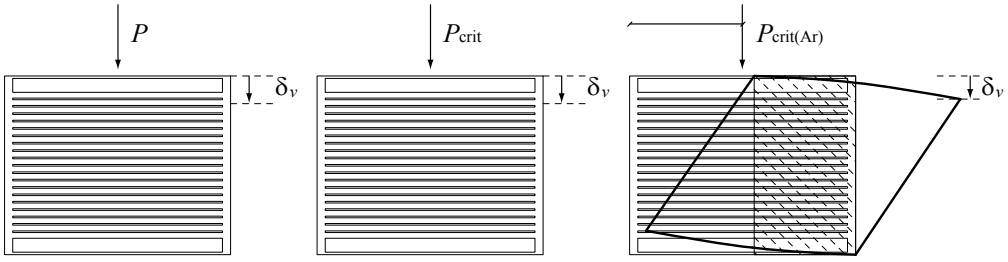

Figure 7. Behavior of the bearing under increasing load. From left to right, steps 1, 2 and 3.

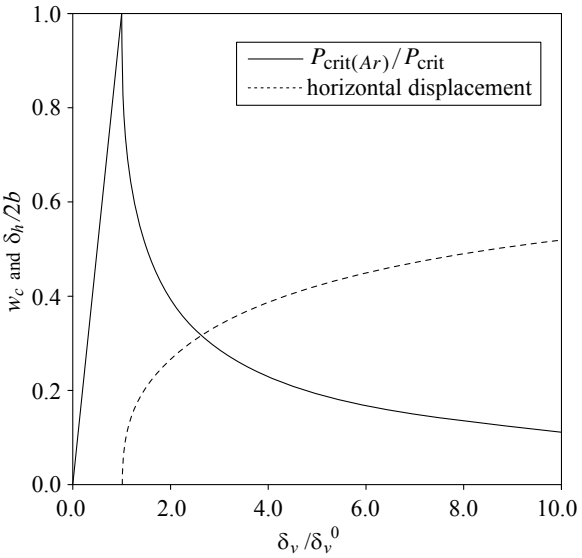

Figure 8. Critical load, horizontal and vertical displacement for an infinite strip bearing.

where I is the actual moment of inertia. The critical load in the undeformed configuration is given by

$$P_{\mathrm{crit}}^0 = \frac{\sqrt{2}}{nt}\pi GASr, \tag{5-3}$$

where the radius of gyration r equals $R/2$. The vertical stiffness of the bearing in the undeflected position is

$$K_v = \frac{E_c A}{nt}, \tag{5-4}$$

so the vertical displacement at the point of buckling is

$$\delta_v = \frac{\pi t}{3\sqrt{2}}. \tag{5-5}$$

As in the case of the strip, this depends only on the thickness of a single layer.

We can assume that (2-2) continues to hold for the circular bearing under lateral displacement and thus the connection between the geometric part of the vertical displacement and the horizontal deformation after buckling will be

$$\delta_v^G = \frac{\pi}{2\sqrt{2}}\frac{t}{R^2}\delta_h^2. \tag{5-6}$$

This is the form the relationship would take if the full circle is taken as the overlap area. When we apply (2-2) to the actual overlap area we need to assume that the horizontal displacement is large enough that some of the parameters of the circular area will need to be modified. For example the factor 6 in the expression for the compression modulus and the one third factor in the effective moment of inertia must be estimated and although we will use the correct shape factor of overlap area, we observe that the shape of the overlap area is intermediate between a strip and a circle and the two corresponding factors for the strip are 4 and 0.2, respectively. In this case then we will use 5 in the estimate of the compression modulus and 0.25 for the effective moment of inertia.

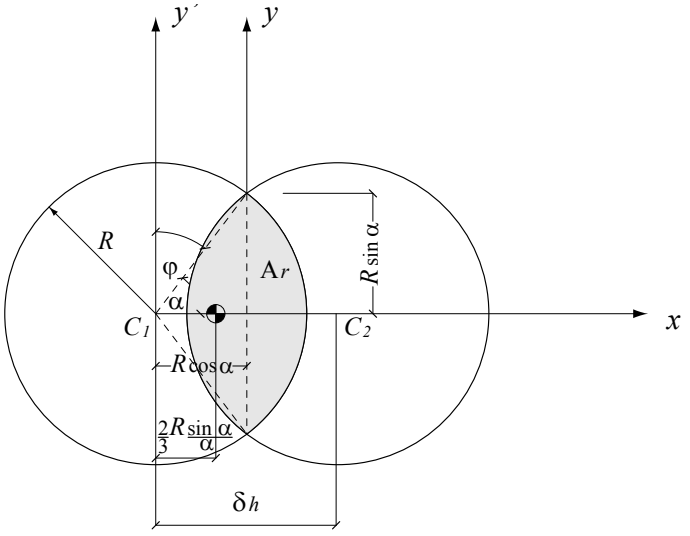

Figure 9. Exact calculation for the overlap area for circular bearing.

5.1. ***Geometrical properties of overlap area.*** The overlap area is given by twice the circular sector centered in the center of the circular bearing subtracted of a triangle as shown in Figure 9 and it is equal to $A_r = 2R^2(\alpha - \sin\alpha\cos\alpha)$. The horizontal displacement of the bearing, d_h, can be expressed as a function of α, in the form $2R\cos\alpha = \delta_h$, giving $\alpha = \arccos(\delta_h/2R)$, and since $\sin\alpha = \sqrt{1-\cos^2\alpha}$, the overlap area becomes

$$A_r = 2R^2\big(\arccos x - x\sqrt{1-x^2}\big), \tag{5-7}$$

with $x = \delta_h/2R$, as plotted in Figure 10, left. In the absence of horizontal displacement ($\delta_h = 0$), we have $\arccos x = \pi/2$, and therefore it is useful to write

$$A_r = \pi R^2\Big(\frac{2}{\pi}\arccos x - \frac{2}{\pi}x\sqrt{1-x^2}\Big).$$

The overlap area length, l_r, is equal to twice $2R\arccos x$, so we can obtain the first shape factor S_r plotted in Figure 10, right, as the ratio between the loaded area and the forced-free area, given by

$$S_r = \frac{2R^2(\alpha - \sin\alpha\cos\alpha)}{4R\alpha t} = \frac{R}{2t}\left(1 - \frac{x\sqrt{1-x^2}}{\arccos x}\right). \tag{5-8}$$

5.2. ***Moment of inertia.*** The moment of inertia for a circular sector with area $R^2\alpha$ is

$$I_{\dot{y}\dot{y}} = \int_0^R \int_{-\alpha}^{\alpha} r\,dr\,d\theta\,(r\cos\theta)^2 = \tfrac{1}{4}R^4\big(\alpha + \tfrac{1}{2}\sin 2\alpha\big). \tag{5-9}$$

Transporting to the centroidal axis, this becomes

$$I_{yy} = \tfrac{1}{4}R^4\big(\alpha + \tfrac{1}{2}\sin 2\alpha\big) - R^2\alpha\Big(\tfrac{2}{3}R\frac{\sin\alpha}{\alpha}\Big)^2, \tag{5-10}$$

and then shifting to the center of the overlap area it becomes

$$I_{yy} = \frac{R^4}{4}\left(\arccos\left(\frac{\delta_h}{2R}\right)\left(1+4\cos^2\frac{\delta_h^2}{4R^2}\right) - \left(1-\frac{\delta_h^2}{4R^2}\right)^{1/2}\frac{\delta_h}{2R}\right). \tag{5-11}$$

Now we take the moment of inertia of a triangle with base $2R\sin\alpha$ and height $R\cos\alpha$ (Figure 9), which is given by $I_{yy}^T = \frac{1}{6}R^4\sin\alpha\cos^3\alpha$, and we subtract it from I_{yy}. This leads to the moment of inertia for the overlap area A_r, given as a function of the lateral displacement by

$$I_{yy(\text{overlap})} = \frac{R^2}{2}\Big(\arccos x(1+4x^2) - (1-x^2)^{1/2}x\left(\tfrac{13}{3}+\tfrac{2}{3}x^2\right)\Big). \tag{5-12}$$

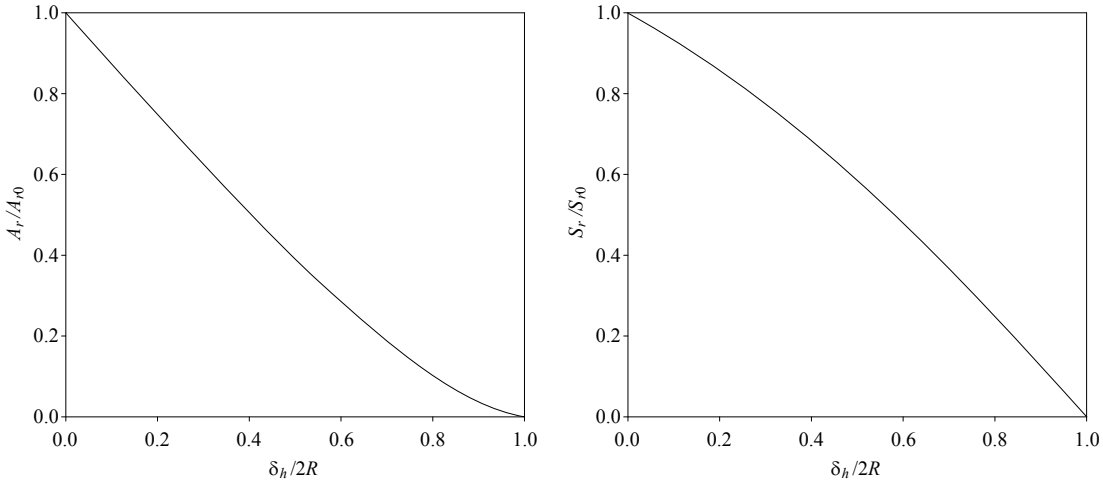

Figure 10. Left: overlap area for increasing lateral displacement. Right: first shape factor for the overlap area.

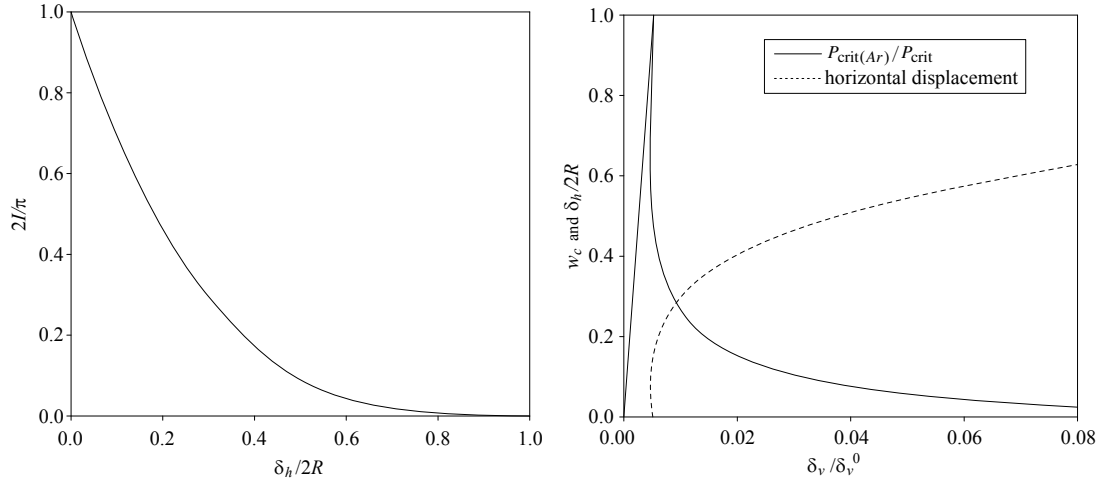

Figure 11. Left: moment of inertia of the overlap area against normalized horizontal displacement. Right: behavior of the bearing with real overlap area.

When the displacement is zero, the bearing is in the undeformed position, so $x = 0$ and $\alpha = \pi/2$, and the moment of inertia is that of a complete circle. On the other hand, when the bearing reaches its maximum horizontal displacement, equal to the diameter $2R$, we have $x = 1$ and $\alpha = 0$. Figure 11, left, shows the function $f(x) = 2I_{yy(\text{overlap})}/\pi$ for $0 < x < 1$.

5.3. ***Vertical displacement.*** The compression modulus can be approximated to $E_c = 5GS^2$ and the effective inertia to $I_{\text{eff}} = \frac{1}{4} I_{yy(\text{overlap})}$, so substituting the values in (2-2), the vertical displacement δ_v^G will be

$$\delta_v^G = R\alpha t\pi \sqrt{\frac{t_r}{5A_r I_{yy(\text{overlap})} h}}\, \delta_h^2. \tag{5-13}$$

To obtain the vertical displacement depending on the load when the bearing moves, we need the critical load on the reduced area, which is $P_{\text{crit}(A_r)} = (G\pi S/2t_r)\sqrt{5A_r I_{yy(\text{overlap})}}$. Thus

$$\delta_v^0 = \frac{P_{\text{crit}(A_r)} t_r}{E_c A_s} = \frac{\pi}{2} \frac{\sqrt{5A_r I_{yy(\text{overlap})}}\, t_r}{5SA_r h}. \tag{5-14}$$

Adding the two terms and simplifying, we get for the total vertical displacement the value

$$\delta_v^t = \delta_v^G + \delta_v^0 = \frac{\pi}{\sqrt{5A_r}} \left(R\alpha t \sqrt{\frac{t_r}{I_{yy(\text{overlap})} h}} \delta_h^2 + \frac{\sqrt{I_{yy(\text{overlap})}}\, t_r}{2h} \right). \tag{5-15}$$

The buckling and post-buckling behavior for the circular bearing with the properties of the overlap area exactly calculated is shown in Figure 11, right.

6. Conclusions

The theoretical analysis has provided estimates of the buckling behavior of bearings that are reinforced with a flexible fiber reinforcement and not bonded to the structure or the foundation. We have shown that the instability of this type of bearing is similar to that of classical imperfection sensitive instability with a buckling load that decreases very rapidly due to the negative infinity of the force displacement curve just after the buckling load is reached.

For example if the vertical displacement is increased to five times that at the point of buckling, the post-buckling load is only 20% of the buckling load. This suggests that this kind of bearing will have to be designed very conservatively. In real terms a bearing made of a rubber compound with a shear modulus $G = 0.70$ MPa (100 psi), a shape factor $S = b/t = 10$ and a second shape factor $S_2 = 2b/(nt) = 2$, the pressure at buckling according to (2-5) is $p_{\text{crit}} = P_{\text{crit}}/(2b) = 2\pi GS^2/(\sqrt{15}\, n)$, which equals 11.2 MPa (1622 psi); this in turn means that the design pressure should be no more than 2.23 MPa (325 psi). This is somewhat less than is used in steel reinforced bearings for large modern isolated buildings but will adequate for low-cost housing and especially for strip bearings supporting masonry wall buildings. We also note that the strip bearings will be arranged in orthogonal directions in the isolation layout as shown in Figure 2 and that only those bearings with their narrow direction in the direction of movement will buckle. In the long direction the bearings are very stable.

References

[Gent and Meinecke 1970] A. N. Gent and E. A. Meinecke, "Compression, bending and shear of bonded rubber blocks", *Polym. Eng. Sci.* **10** (1970), 48–53.

[Imbimbo and Kelly 1997] M. Imbimbo and J. M. Kelly, "Stability aspects of elastomeric isolators", *J. Earthquake Spectra* **13** (1997), 431–449.

[Kelly 1997] J. M. Kelly, *Buckling behaviour of elastomeric bearings in earthquake-resistant design with rubber*, 2nd ed., Springer, London, 1997.

[Kelly 1999] J. M. Kelly, "Analysis of fiber-reinforced elastomeric isolators", *J. Earthquake Eng.* **2** (1999), 19–34.

[Kelly 2002] J. M. Kelly, "Seismic isolation systems for developing countries", *J. Earthquake Spectra* **18** (2002), 1150–1157.

[Kelly 2003] J. M. Kelly, "Tension buckling in multilayer elastomeric bearings", *J. Eng. Mech.* **129** (2003), 1363–1368.

[Kelly and Takhirov 2002] J. M. Kelly and S. M. Takhirov, "Analytical and experimental study of fiber-reinforced strip isolators", Report 2002-11, Earthquake Engineering Research Center, University of California, Berkeley, 2002, available at http://nisee.berkeley.edu/elibrary/Text/1278634.

[Kelly and Takhirov 2004] J. M. Kelly and S. M. Takhirov, "Analytical and numerical study on buckling of elastomeric bearings with various shape factors", Report 2004-03, Earthquake Engineering Research Center, University of California, Berkeley, 2004, available at http://nisee.berkeley.edu/elibrary/Text/1293197.

[MARC 1988] *MARC General-purpose finite element program*, MARC Analysis Research Corporation, Palo Alto, CA, 1988.

[Marsico 2008] M. R. Marsico, *Seismic isolation and energy dissipation: theoretical basis and applications*, Ph.D. thesis, Università di Napoli Federico II, Napoli, 2008, available at http://tinyurl.com/MarsicoThesis-pdf.

[Marsico and Kelly 2009] M. R. Marsico and J. M. Kelly, "Stability and post-buckling behaviour in non-bolted elastomeric isolators", pp. no. 226 in *Proceedings of the XIII Italian Conference on Earthquake Engineering* (ANIDIS) (Bologna, 2009), 2009. On CD.

[Tsai and Kelly 2002] H. C. Tsai and J. M. Kelly, "Stiffness analysis of fiber-reinforced rectangular isolators", *J. Eng. Mech.* **128** (2002), 462–470.

[Tsai and Kelly 2005a] H. C. Tsai and J. M. Kelly, "Buckling load of seismic isolators affected by flexibility of reinforcement", *Int. J. Solids Struct.* **42** (2005), 255–269.

[Tsai and Kelly 2005b] H. C. Tsai and J. M. Kelly, "Buckling of short beams with warping effect included", *Int. J. Solids Struct.* **42** (2005), 239–253.

[UBC 2007] *Uniform Building Code*, International Code Council, 2007.

Received 9 Mar 2010. Accepted 30 Sep 2010.

JAMES M. KELLY: jmkelly@berkeley.edu
Pacific Earthquake Engineering Research Center, University of California, Berkeley, 1301 South 46th Street Building 452, Richmond, CA 94804-4698, United States

MARIA ROSARIA MARSICO: m.r.marsico@bristol.ac.uk
Department of Mechanical Engineering, University of Bristol, Bristol, BS8 1TH, United Kingdom

SEISMIC ISOLATION AND PROTECTIVE SYSTEMS

http://pjm.math.berkeley.edu/siaps/

See inside back cover or http://www.jomms.org for submission guidelines.

SIAPS (ISSN 2150–7902) is published in electronic form only. The subscription price for 2010 is US $150/year. Subscriptions, requests for back issues, and changes of address should be sent to Mathematical Sciences Publishers, Department of Mathematics, University of California, Berkeley, CA 94720–3840.

SIAPS peer-review and production is managed by EditFLOW™ from Mathematical Sciences Publishers.

PUBLISHED BY
mathematical sciences publishers
http://www.mathscipub.org
A NON-PROFIT CORPORATION
Typeset in LaTeX

Seismic Isolation and Protection Systems vol 1, no 1, 2010

2150-7902(2010)1:1;1-G